Ion temperature and gas pressure effects on the magnetized sheath dynamics during plasma immersion ion implantation

M. Khoram, H. Ghomi, and N. Navab Safa

Citation: Physics of Plasmas **23**, 033511 (2016); doi: 10.1063/1.4944503
View online: http://dx.doi.org/10.1063/1.4944503
View Table of Contents: http://scitation.aip.org/content/aip/journal/pop/23/3?ver=pdfcov
Published by the AIP Publishing

Ion temperature and gas pressure effects on the magnetized sheath dynamics during plasma immersion ion implantation

M. Khoram,[1,a)] H. Ghomi,[2,b)] and N. Navab Safa[2,c)]
[1]Department of Physics, Borujerd Branch, Islamic Azad University, Borujerd, Iran
[2]Laser and Plasma Research Institute, Shahid Beheshti University, Evin, 1983963113 Tehran, Iran

(Received 22 May 2015; accepted 7 March 2016; published online 21 March 2016)

Here, a collisional magnetized plasma with finite ion temperature is considered to examine the effects of the ion temperature and gas pressure on the plasma-sheath dynamics. We use the two-fluid model of plasma-sheath where the nonlinear equations of a dynamic sheath are solved using a full implicit scheme of finite difference method along with some convenient initial and boundary conditions at the plasma center and target. It is found that the ion temperature only has a significant effect on the characteristics of low voltage sheath, while the gas pressure (collision rate) seriously affects the dynamic characteristics of the low and high voltage plasma-sheath. One can see, increasing the ion temperature in low voltage plasma-sheath causes to increase the temporal curve of the ion dose and the ion impact energy on the target, reduces the temporal curve of the sheath width, and has no any effect on the temporal curve of the ion incident angle on the target. However, rising the gas pressure in low and high voltage plasma-sheath reduces all of these temporal curves. © *2016 AIP Publishing LLC*. [http://dx.doi.org/10.1063/1.4944503]

I. INTRODUCTION

Plasma Immersion Ion Implantation (PIII)[1,2] has been shown to be an effective technique for semiconductor fabrication and material processing.[3–6] It emulates conventional ion-beam ion implantation (IBII) in a number of areas. For example, it has high sample throughput (high current density) and it is a paralleled processing technique in which the implantation time is independent of the wafer size. It also obviates the line-of-sight restriction imposed by IBII.

In PIII, accurate knowledge of the incident ion dose is very critical to the success of the process. The dynamic sheath model plays a very important role in PIII processes because it is used to predict process parameters and implantation results including the implant doses and energies. The optimum characteristics of plasma system can be determined from the sheath dynamic analysis. Unfortunately, accurate modeling and prediction of the implantation dose in PIII are quite difficult because it is a complicated function of interrelated processing conditions such as plasma density, pulse duration, accelerating voltage, external magnetic field, ion mass, temperature, and charge state, yet the same dose can be obtained using another set of implantation parameters.

The physics of plasma sheath is still not perfectly understood, because it is a nonlinear medium with a large set of parameters. Plasma sheaths become even more complicated for time-dependent problems, such as sheaths in Radio Frequency (RF) glow discharges and pulsed discharges. There has recently been an explosion of interest in the behavior of plasma-sheaths which is formed at an electrode biased with a pulsed negative voltage. This problem is of special interest in PIII technology, where ions are extracted from plasma, accelerated by a high potential drop in the sheath, and injected into the surface layer of a material being treated.

In a simple model of PIII, the confined homogeneous plasma is brought in contiguity with a flat conducting electrode or target. A series of negative, high-voltage pulses are applied to the electrode to implant ions into the electrode. As a result, electrons are repelled from the electrode and move back into the plasma leaving a positive ion sheath. Ions remain stationary resulting in a so-called ion matrix sheath.[7–9] This initial sheath is formed on a time scale of the order of $1/\omega_p$ (where ω_p is the electron plasma frequency). At a characteristic time scale of the order of $1/\Omega_p$ (where Ω_p is the ion plasma frequency), ions start falling towards the target (electrode). Therefore, the sheath edge, where quasi-neutrality breaks down, propagates into the plasma and a rarefactive ion distribution begins to propagate into the sheath. Thickness of the time-dependent collisionless sheath is given by[10]

$$d(t) = d_0\left(\frac{2}{3}\,\Omega_p\, t + 1\right)^{1/3}, \tag{1}$$

where $d_0 = \sqrt{2\varepsilon_0 V_T/en_0}$ is the thickness of the ion matrix sheath, V_T is the applied negative voltage to the target, ε_0 is the free space permittivity, and e is the unit of electric charge.

Already, Minghao *et al.*[11] have investigated the ion temperature effect on collisional and collisionless RF sheath dynamic. They found that the ion temperature has significant effects on the characteristics of the collisional RF sheath. They have solved plasma fluid equations from plasma center to the wall (biased with a low voltage sinusoidal source) and presented their results in time-averaged form. Das *et al.*[12] studied the low voltage DC sheath formation in a thermal

a)Email: m.khoramabadi@srbiau.ac.ir
b)Email: h-gmdashty@sbu.ac.ir
c)Email: n_navabsafa@sbu.ac.ir

plasma. They have solved the steady state fluid equations of sheath from plasma-sheath edge to the wall as boundaries of the plasma-sheath, using a Bohm criteria obtained by themselves. Alterkop[13] has studied the steady state DC plasma sheath formation in a thermal plasma using his own special approximations. We have also perused the ion temperature effect on the steady state sheath structure and the Bohm criterion in the collisional warm plasma.[14–17] Safa *et al.*[18] have investigated the sheath dynamics and implantation profiles during the PIII process on a long step shaped target in the presence of an external DC magnetic field and showed that the magnetic field inclination angle strongly affects the ion implanted dose and ion energy on the target surfaces.

In this paper, we will computationally study the PIII process for different ion temperatures and neutral gas pressures to investigate the influence of ion temperature and ion-neutral collision on the dynamic characteristics of a pulsed collisional magnetized sheath. We have used an external magnetic field in our model to be able to control the ion incident angle on the target. The normalized potential, ion density, sheath width, incident dose, incident angle, and impact energy of ions on the target surface will be analyzed. Here, we use a fluid model to investigate the time evolution of an expanding sheath into the plasma. The model equations are solved through an implicit finite difference scheme.[19] Despite of the explicit scheme, in the implicit scheme one has to solve $n_x N$ equations simultaneously in each time step, in which n_x is the number of space steps and N is the number of equations. In this paper, we have done the thermal and collisional discussions on the temporal curve of the target characteristics. To do this, the low and high voltage pulsed plasma-sheaths have been separately discussed. Different thermal and collisional parameters are the other differences between this paper and the previous works.

After introduction, in Section II, a collisional magnetized plasma with thermal ions is formulated and the convenience initial and boundary conditions are nominated. Numerical results and their explanation are presented in Section III. Section IV gives a summary and conclusions.

II. BASIC EQUATIONS AND SHEATH FORMULATION

The implantation geometry is schematically displayed in Fig. 1. An active collisional magnetized plasma with finite ion temperature limited at one side by a conducting flat electrode or target is considered to discuss the formation of dynamic plasma-sheath. The position of the target is taken at $x=0$. We assume at the initial time $t=0$, the plasma which is located at the $x>0$ has filled with stationary singly charged ions and the charge neutrality condition $n_i=n_e=n_0$ is fulfilled there.

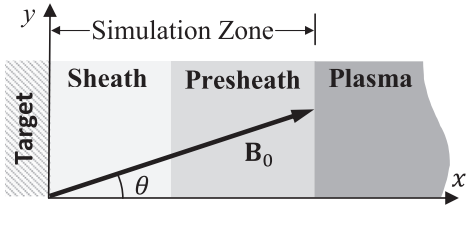

FIG. 1. The plasma-sheath-target configuration in the magnetized PIII.

At the moment $t=0^+$, the bias on the target is switched on from $V=0$ to a negative bias $V_T(t)$, drawing ions to the target and repelling electrons to the plasma. Under this condition, a non neutral plasma so called the plasma-sheath is formed around the target.

On the other hand, far from the plasma-sheath, there is a thermal plasma with ion and electron temperatures T_i and T_e, respectively, where the electric potential is $V=0$ and is separated from the sheath by a semi-neutral attenuate presheath. The singly charged ions are formulated by a fluid model in the sheath and presheath regions.[20–24] Then, distributions of the ion density, ion velocity, and electric potential in the sheath evolve self consistently in time. In the quiescent presheath and sheath of a plasma with sufficiently low pressure, the continuity and motion equations of the ions supplemented by the pressure and collisional terms are

$$\frac{\partial n_i}{\partial t}+\nabla\cdot(n_i\mathbf{v})=0, \tag{2}$$

$$mn_i\left(\frac{\partial}{\partial t}+\mathbf{v}\cdot\nabla\right)\mathbf{v}=en_i(\mathbf{E}+\mathbf{v}\times\mathbf{B})-\nabla p_i-mn_i\nu\mathbf{v}, \tag{3}$$

where $\mathbf{E}=-\nabla V$ (with V as the electric potential) is the electric field, and m, $\mathbf{v}$, ν, and p_i are the mass, velocity, collision frequency, and pressure of ion, respectively.

Also, the electrons are in the electrostatic potential well of the target and are assumed to be in thermal equilibrium, so their density n_e obeys the Boltzmann relation

$$n_e=n_0\exp\left(\frac{eV}{k_BT_e}\right), \tag{4}$$

where k_B is the constant of Boltzmann.

Finally, the set of equations to be solved is completed by Poisson's equation which relates the electric potential to the electron and ion densities as follows:

$$\nabla^2V=-\frac{e}{\varepsilon_0}(n_i-n_e). \tag{5}$$

On the basis of the above equations, the ion state equation $p_i=k_BT_in_i$, the ion thermal flow equation $p_i=c\,n_i^{\gamma}$ (with γ as the ion polytrophic coefficient), and the ion-neutral collision frequency $\nu=n_g\sigma_s v(v/c_s)^{\beta}$ (where $n_g=P_g/k_BT_g$, P_g and T_g are the density, pressure, and temperature of neutral gas, respectively, σ_s is the ion-neutral collision cross section in the sound velocity c_s, and β, so called the collision power parameter, is a real number between -1 and 0 that $\beta=-1$ introduces the collision with constant frequency, while $\beta=0$ presents the collision with constant mean free path), one can describe the dynamic structure of plasma sheath around target.

Before normalizing the main equations (2)–(5), using the state and thermal flow equations of ion and omission the constant c between them, one can find the ion thermal force as follows:

$$\nabla p_i=\gamma k_BT_i\left(\frac{n_i}{n_0}\right)^{\gamma-1}\nabla n_i. \tag{6}$$

For the sake of convenience, it is efficient to introduce some normalized parameters and variables

$$N_i = \frac{n_i}{n_0}, \quad N_e = \frac{n_e}{n_0}, \quad T = \frac{T_i}{T_e}, \quad \mathbf{X} = \frac{\mathbf{x}}{\lambda_D},$$

$$\Omega_c = \frac{eB}{m}, \quad \Omega_p = \sqrt{\frac{n_0 e^2}{m\varepsilon_0}}, \quad \alpha = \frac{\lambda_D}{\lambda} = \lambda_D n_g \sigma_s,$$

$$\Omega = \frac{\Omega_c}{\Omega_p}, \quad \tau = \Omega_p t, \quad c_s = \sqrt{\frac{k_B T_e}{m}} = \lambda_D \Omega_p,$$

$$\phi = \frac{eV}{k_B T_e}, \quad \lambda_D = \sqrt{\frac{\varepsilon_0 k_B T_e}{n_0 e^2}}, \quad u_j = \frac{v_j}{c_s} (j = x, y, z),$$

where Ω is the ratio of the ion cyclotron frequency Ω_c to the ion plasma frequency Ω_p. Indeed, Ω_c introduces a vector paralleled to the magnetic field $\mathbf{B} = B_0(\cos\theta_0\,\hat{\mathbf{x}} + \sin\theta_0\,\hat{\mathbf{y}})$ with the magnitude eB_0/m. T is the ion to electron temperature ratio, τ is the normalized time by $1/\Omega_p$, ϕ is the electric potential normalized by $k_B T_e/e$, α is the ion-neutral collision parameter, $\lambda = 1/n_g\sigma_s$ is the mean free path of ion collision, u is the ion velocity normalized by the ion sound velocity c_s, N_i and N_e are the ion and electron densities, respectively, normalized by n_0, and X is the space coordinate normalized by Debye length λ_D. Since the target is planar, $\nabla \to (\partial/\partial X)\hat{\mathbf{x}}$ and the normalized one-dimensional form of Equations (2)–(5) will be as follow:

$$\frac{\partial N_i}{\partial \tau} + \frac{\partial (N_i u_x)}{\partial X} = 0, \tag{7}$$

$$\left(\frac{\partial}{\partial \tau} + u_x \frac{\partial}{\partial X}\right)\mathbf{u} = -\frac{\partial \phi}{\partial X}\,\hat{\mathbf{x}} + \mathbf{u} \times \Omega - \gamma T N_i^{\gamma-2} \frac{\partial N_i}{\partial X}\,\hat{\mathbf{x}} - \alpha u^{\beta+1}\,\mathbf{u}, \tag{8}$$

$$N_e = \exp(\phi), \tag{9}$$

$$\frac{\partial^2 \phi}{\partial X^2} = N_e - N_i. \tag{10}$$

Using the definition $\Omega = eB_0(\cos\theta_0\hat{\mathbf{x}} + \sin\theta_0\hat{\mathbf{y}})/m\Omega_p = \Omega_0(\cos\theta_0\hat{\mathbf{x}} + \sin\theta_0\hat{\mathbf{y}})$, one can rewrite the vector equation (8) in the scalar form to find

$$\left(\frac{\partial}{\partial \tau} + u_x \frac{\partial}{\partial X}\right)u_x = -\frac{\partial \phi}{\partial X} - \Omega_0 u_z \sin\theta_0 - \gamma T N_i^{\gamma-2}\frac{\partial N_i}{\partial X} - \alpha u^{\beta+1} u_x, \tag{11}$$

$$\left(\frac{\partial}{\partial \tau} + u_x \frac{\partial}{\partial X}\right)u_y = \Omega_0 u_z \cos\theta_0 - \alpha u^{\beta+1} u_y, \tag{12}$$

$$\left(\frac{\partial}{\partial \tau} + u_x \frac{\partial}{\partial X}\right)u_z = \Omega_0 u_x \sin\theta_0 - \Omega_0 u_y \cos\theta_0 - \alpha u^{\beta+1} u_z. \tag{13}$$

Eqs. (7) and (9)–(13) make a complete set of equations describing the dynamic structure of plasma-sheath. We solve the equations in a region from the plasma center to the target supplied by a negative high voltage introduced by

$$V_T(t) = V_P\left[1 - \exp\left(-\frac{t}{t_r}\right)\right], \tag{14}$$

in which V_P and t_r are the voltage amplitude and rise time of pulse, respectively. In order to examine the dynamic structure of plasma-sheath and investigate the plasma parameters effect such as the ion temperature on the sheath dynamic structure, the complete set of equations are numerically solved using a second-order finite difference scheme in space and a first-order finite difference scheme in time. After discretization of equations in full implicit finite difference scheme, some linearization is required. In order to linearize the equations in time, we used Taylor's expansion approximation $f(t + \triangle t) \approx f(t) + (\partial f(t)/\partial t)\triangle t$ (see the Appendix).

III. COMPUTATIONAL RESULTS AND DISCUSSION

In order to solve Equations (7) and (9)–(13) and to find the time-space dependence of ϕ, u_x, u_y, u_z, and N_i, some proper initial and boundary conditions are necessary. The boundary conditions in the plasma center and on the target for the time interval $0 < \tau < \tau_p$ are

$$u_x(L,\tau) = u_y(L,\tau) = u_z(L,\tau) = 0,$$
$$\phi(0,\tau) = \phi_T(\tau),\ \phi(L,\tau) = 0,\ N_i(L,\tau) = 1,$$

where $\tau_p = \Omega_p t_p$ is the normalized pulse duration, $\phi_T = eV_T/k_B T_e$ is the normalized voltage of target, and L is the normalized length of simulation region and introduces the location of a point in the plasma, sufficiently far from the target that is called the plasma center. Also, the initial conditions for the space interval $0 < X < L$ are

$$\phi(X,0) = 0, \quad N_i(X,0) = 1,$$
$$u_x(X,0) = u_y(X,0) = u_z(X,0) = 0.$$

The normalized equations can now be solved assuming some constant parameters. Atomic nitrogen is used as the ion that should be implanted on the target surface. Nitrogen implantation of steel surfaces by PIII has shown to improve mechanical properties and corrosion performance.[25,26] Nitrogen plasma density is assumed $n_0 = 10^{14}\,\mathrm{m}^{-3}$ ($\Omega_p = 3.5260 \times 10^6$ Hz), electron temperature $T_e = 1$ eV, the ion polytrophic coefficient $\gamma = 1$ (for isothermal current of ions), the collision power number $\beta = -1$ (for constant collision frequency), rise time $t_r = 0.1t_p$, magnetic field amplitude $B_0 = 0.2$ T ($\Omega_c = 3.4400 \times 10^6$ Hz), and the magnetic field deviation angle $\theta_0 = \pi/3$. According to the assuming data, one can find $\lambda_D = 744.3\,\mu$m and $c_s = 2624.3$ m/s.

We alter the gas pressure $P_g = k_B T_g n_g$ (that is, in direct relation to the collision parameter α) and the ion temperature T_i to examine their effects on the sheath dynamic structure. Calculations show that the ion temperature effect is a function of the target bias voltage. So, we should consider two different situations: low voltage sheath defined by $-100\,\mathrm{V} \le V_T \le 0$ and high voltage sheath defined by $V_T \le -100$ V. It is clear that the low voltage sheath is never used in the PIII, and we have proposed it here to present a comprehensive discussion.

A. Low voltage dynamic sheath

In the low voltage sheath, ion temperature plays a significant role on the dynamic structure of plasma-sheath. To study the dynamic structure of low voltage sheath, we have numerically solved the complete set of equations assuming $\phi_p = eV_p/k_B T_e = -15$, $\Delta\tau = \Omega_p \Delta t = 10^{-4}$ as the normalized time steps, $n_t = 120\,000$ as the total number of time steps, $\Delta X = \Delta x/\lambda_D = 0.5$ as the normalized space steps, and $n_x = 100$ as the total number of space steps. Using the time and space data, one can find the pulse duration $t_p = n_t \Delta t = 3.4033\,\mu s\,(\tau_p = 12)$ and the simulation width $L_x = n_x \Delta x = 3.7215\,\text{cm}$ $(L = 50)$. Variable parameters are the ion temperature and gas pressure which include the values $T_i = 0$, 0.5, and 1.0 eV, and $P_g = 0$ and 0.1 Pa. The simulation results have been shown in Figs. 2–5.

Figure 2 displays temporal curves of the ion current density $J_x = en_i u_x$ perpendicular to the target for some different ion temperatures and gas pressures. From this figure, one can see that the temporal curve of the ion current density increases from zero to a maximum value, afterward, it decreases and saturates to a constant value. This figure shows that the ion temperature increases the maximum and the saturation values of the temporal curve of ion current density. Also, the maximum and the saturation values of the temporal curve of ion current density are decreased by the gas pressure. On the other hand, since the ion dose is in direct connection with the ion current density, their temporal curves have the same dependency on the ion temperature and gas pressure.

Here, sheath width is defined as the distance between target and the plasma-sheath interface, that is, the point in which the normalized electric potential reduces to $\phi = -0.01$. Figure 3 exhibits temporal curves of the sheath width normalized by Debye length $\lambda_D = 0.744\,\text{mm}$ for some different values of the ion temperature and gas pressure. This figure shows that the sheath width is a descending function of the both parameters gas pressure and ion temperature. In other words, increasing the ion temperature and gas pressure reduces the plasma-sheath width.

Ion incident angle is defined as the angle between ion velocity and normal vector on the target surface. It is then calculated via $\arctan\left(\sqrt{u_y^2 + u_z^2}/u_x\right)$. We know that the ion

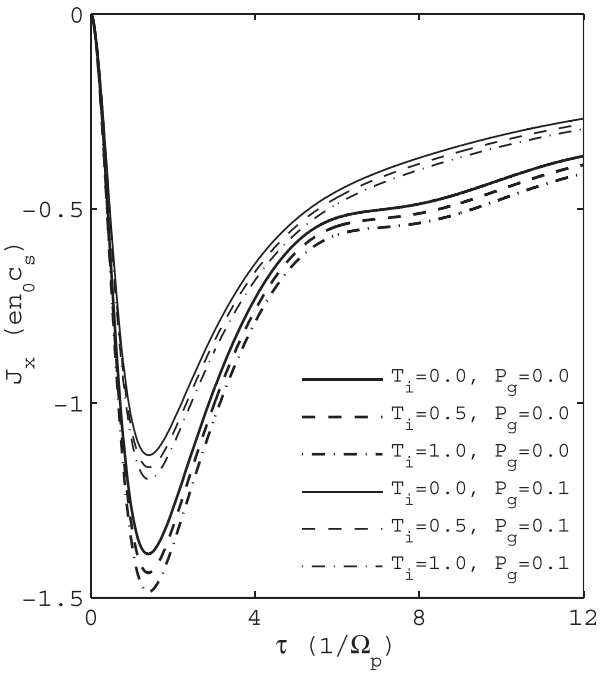

FIG. 2. Temporal variations of the ion current density J_x normalized by $J_0 = en_0 c_s = 0.0786\,\text{A/m}^2$ as a function of the ion temperature T_i and gas pressure P_g. The simulation parameters are $\phi_p = -15$, $\tau_p = 12$, and $L = 50$.

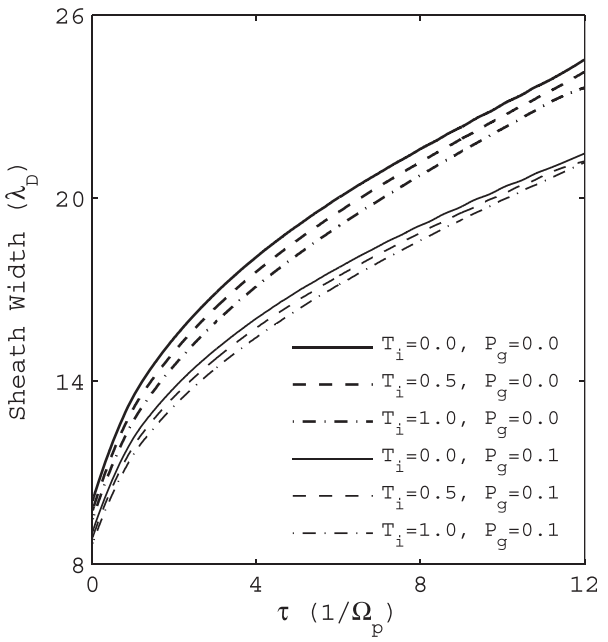

FIG. 3. Temporal curve of the sheath width normalized by Debye length $\lambda_D = 0.744\,\text{mm}$ as a function of the ion temperature T_i and the gas pressure P_g. The constant parameters are the same as Fig. 2.

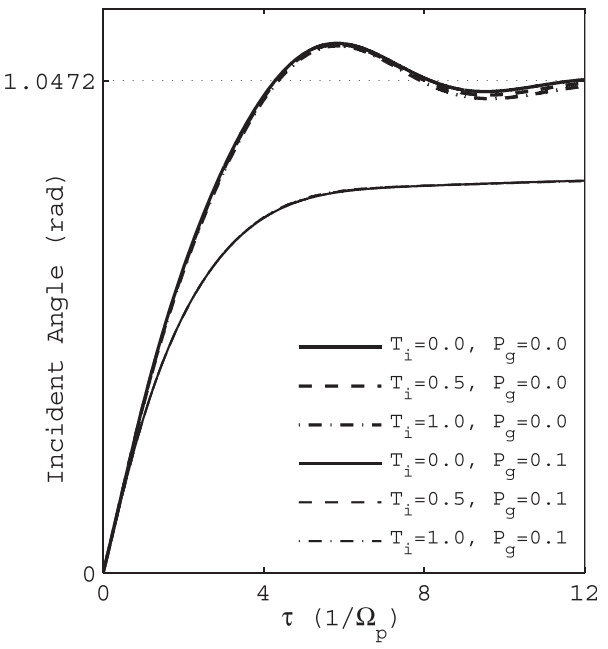

FIG. 4. Temporal curve of the ion incident angle on the target surface as a function of the ion temperature T_i and gas the pressure P_g. The constant parameters are the same as Fig. 2.

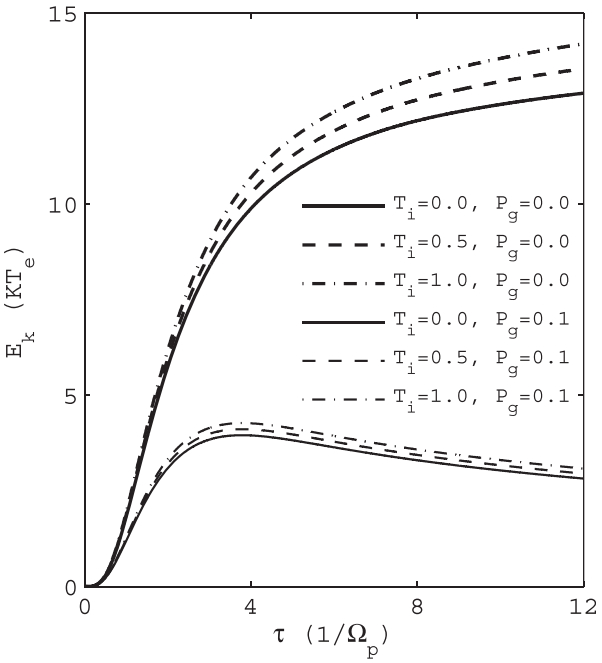

FIG. 5. Temporal curve of the ion impact energy normalized by $k_BT_e = 1$ eV as a function of the ion temperature T_i and the gas pressure P_g. The constant parameters are the same as Fig. 2.

vertical incident on the target increases the ion penetration into the target, while the ion oblique incident decreases the ion penetration into the target and grows up the sputtering of the target. Temporal curves of the ion incident angle have been depicted in Fig. 4. This figure shows that the ion incident angle on the target begins to increase from zero over time and after some fluctuations caused by magnetic field is saturated to a constant value. In the absence of collision ($P_g = 0$), the constant incident angle is approached to the magnetic field deviation angle $\theta_0 = \pi/3 = 1.0472$ rad. It means that the ion velocity on the target is paralleled to the external magnetic field.

As a result, the magnetic force and fluctuations caused by the magnetic field will be disappeared as soon as the ion velocity is constantly paralleled the magnetic field. Increasing the ion temperature has a weak effect on the ion incident angle and will negligibly reduce the ion saturated incident angle. According to Fig. 4, the gas pressure reduces the ion saturated incident angle. It means that in order to control the ion incident angle on the target by DC magnetic field, feeding gas should be sufficiently dilute.

Temporal curves of the ion impact energy defined by $E_k = m(v_x^2 + v_y^2 + v_z^2)/2 = k_BT_e(u_x^2 + u_y^2 + u_z^2)/2$ have been displayed in Fig. 5 for some different ion temperatures and gas pressures. Fig. 5 shows that the ion impact energy on the target surface increases from zero and is eventually saturated to a constant value. The ion saturated energy on the target increases by ion temperature and reduces by gas pressure. As one can see, the ions on the target never gain the full energy of the sheath electric potential difference even in the absence of collision. The reason is that the sheath expanding time is too short (on the order of $1/\omega_p$) with respect to the ion transit time across the sheath (on the order of $1/\Omega_p$), and the sheath potential difference varies during the ion flight across the sheath. In other words, displacement current across the expanding sheath leads to an increase in the ion implanted current and causes to a decrease in the implanted ion energy with respect to the stationary sheath with the same parameters.[27,28]

Generally, Figs. 2–5 show that the gas pressure reduces fluctuations induced by the magnetic field in the temporal curves. Also, the gas pressure reduces the ion temperature effects on the curves.

B. High voltage dynamic sheath

Although ion temperature has significant effects on the low voltage sheath dynamic structure, it has negligible effect on the high voltage sheath dynamic structure. In the high voltage plasma sheath, the thermal force term in the ion motion equation is weak because when we changed the ion temperature, temporal curve of the target characteristics did not change. Indeed, the ion thermal force according to Eq. (6) is composed of the ion temperature and the ion density gradient, and none of these factors depends on the pulsed voltage applied to the target. Then, despite of the other terms in the ion motion equation, the ion thermal term remains unchanged in low and high voltage sheaths.

To study the dynamic structure of high voltage sheath, we have solved the dynamic equations (7) and (9)–(13) and have assumed $\phi_p = -15000$, $\Delta\tau = 10^{-3}$, $n_t = 40\,000$, $\Delta X = 0.5$, and $n_x = 1000$. It is clear that the pulse duration and simulation space will be $t_p = 11.3443\,\mu$s ($\tau_p = 40$) and $L_x = 37.2150$ cm ($L = 500$), respectively. Variable parameter is just gas pressure which includes the values $P_g = 0$, 0.3, 0.6, 0.9, 1.2, and 1.5 Pa. Simulation results have been summarized in Figs. 6–9. In these figures, we have analyzed the gas pressure effects more precise than the previous figures.

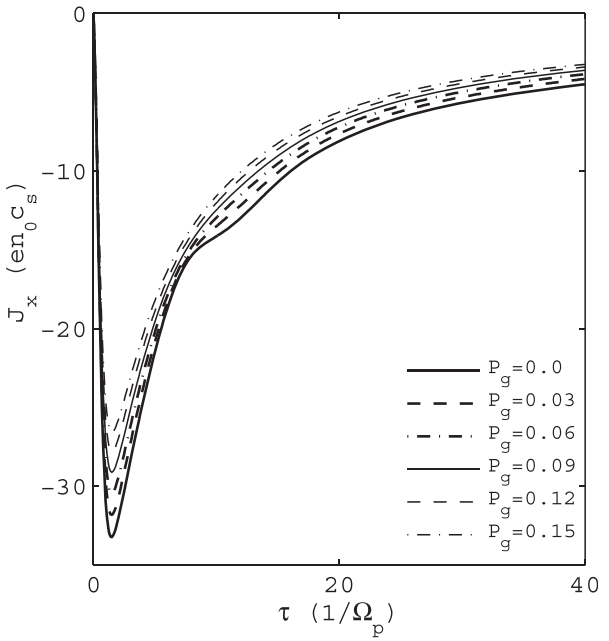

FIG. 6. Temporal curve of the ion current density J_x normalized by $J_0 = 0.0786$ A/m^2 as a function of the gas pressure P_g. The simulation constant parameters are $\phi_p = -15000$, $\tau_p = 40$, and $L = 500$.

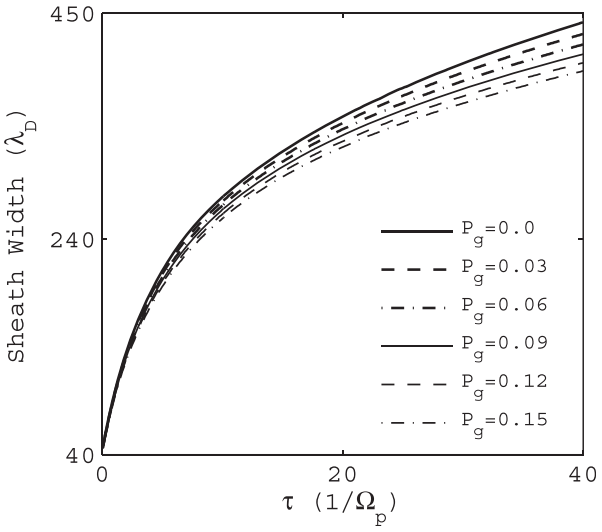

FIG. 7. Temporal curve of the plasma-sheath width normalized by Debye length $\lambda_D = 0.744$ mm as a function of the gas pressure P_g. The constant parameters are the same as Fig. 6.

Figure 6 displays temporal curves of ion current density J_x for some different gas pressures in high voltage sheath. It has the same temporal variations as Fig. 2. This figure shows that the gas pressure decreases the maximum and saturated values of the ion current density on the target. It ensures that the ion dose on the target is a descending function of the gas pressure and a rising function of the plasma density. Therefore, the ion dose and ion current density are obviously in direct connection with the plasma ionization rate. The experimental observations confirm our numerical results.[29,30]

Figure 7 exhibits temporal curves of plasma-sheath width normalized by Debye length $\lambda_D = 744.3\ \mu$m for some different values of the gas pressure. According to Fig. 7, the plasma-sheath width instantly grows up to the matrix sheath width $D_0 = d_0/\lambda_D \approx 40$ and then, it begins to increase in accordance to relation (1). It is clear from this figure that by increasing the gas pressure, one can reduce the plasma-sheath width in PIII.

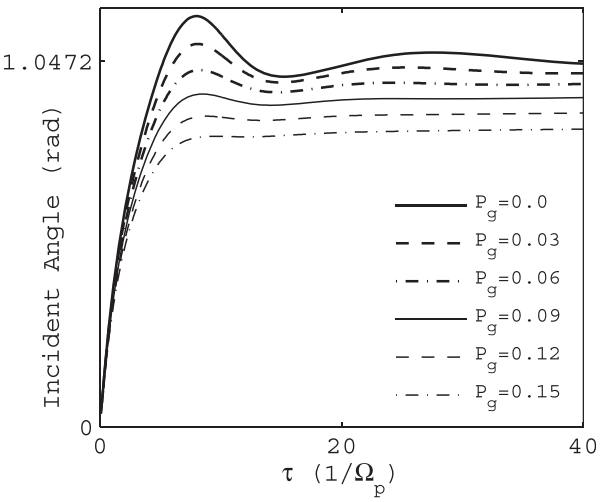

FIG. 8. Temporal curve of the ion incident angle on the target surface as a function of the gas pressure P_g. The constant parameters are the same as Fig. 6.

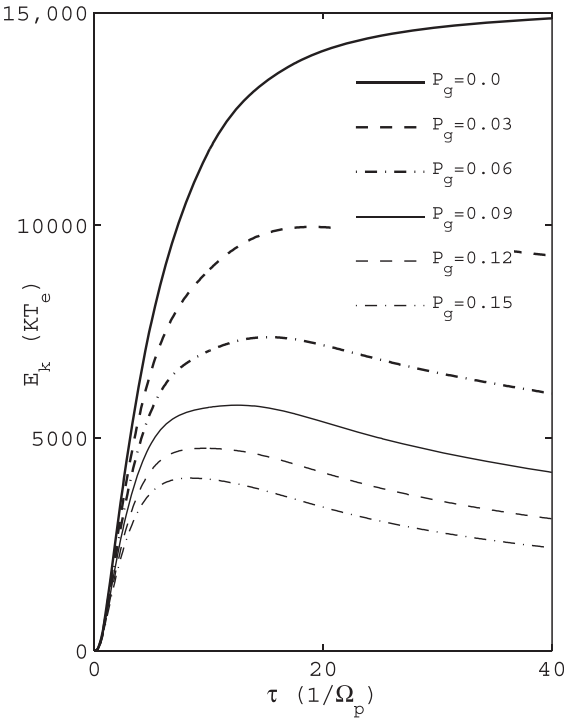

FIG. 9. Temporal curve of the ion impact energy normalized by $k_B T_e = 1$ eV as a function of the gas pressure P_g. The constant parameters are the same as Fig. 6.

Temporal curves of the ion incident angle have been depicted in Fig. 8 for some different gas pressures P_g. This figure shows that the ion incident angle on the target begins to increase from zero and after some fluctuations caused by the magnetic field is saturated to a constant value. In the absence of collision ($P_g = 0$), the constant incident angle is approached to the magnetic field deviation angle θ_0. It means that the ion velocity at the target surface has been paralleled to the external magnetic field. According to Fig. 8, the gas pressure decreases the ion saturated incident angle. It means, increasing the gas pressure reduces the magnetic control on the ion incident angle on the target.

Fig. 9 displays temporal curves of the ion impact energy E_k normalized by $k_B T_e = 1$ eV as a function of the gas pressure. This figure shows the same variations as Fig. 5 in the low voltage sheath. As one can see, gas pressure leads to a decrease in the ion saturated impact energy. As it was quoted about the low voltage sheath, the ions never gain the full energy of the target bias voltage even in the absence of collision. We can expect that the ion impact energy gains the full energy of the target bias voltage after full stability of the dynamic sheath. These results are in good agreement with the experimental data.[29,30]

IV. SUMMARY AND CONCLUSIONS

To investigate influence of the ion temperature and gas pressure on the dynamic behavior of plasma sheath in the PIII process, we have used the fluid model of plasma and numerically solved time dependent equations of a pulsed magnetized plasma-sheath through an implicit finite difference scheme. Temporal curves of some plasma-sheath

characteristics such as normalized current density, incident angle, and impact energy of ions on the target surface as well as sheath width were presented in the both of low and high voltage sheaths.

In the low voltage dynamic sheath, ion temperature plays a significant role on the dynamic structure of plasma-sheath. Calculations show that temporal curves of the ion current density in the sheath grow up by increasing the ion temperature and decreasing the gas pressure. Sheath width is a descending function of the both parameters gas pressure and ion temperature. Temporal curves of the ion incident angle on the target begin to increase from zero and after some fluctuations caused by magnetic field are saturated to a constant value. This saturated incident angle is the same as the magnetic field deviation angle $\theta_0 = \pi/3 = 1.0472$ rad in the absence of collision. It means that the magnetic force will be disappeared over time. Ion temperature has a weak effect on the temporal curve of the ion incident angle, but the gas pressure decreases the temporal curve of the ion incident angle. The ion impact energy on the target surface grows up from zero and is saturated to a constant value over time. The ion saturated impact energy is increased by ion temperature and is reduced by gas pressure. Also in the dynamic sheath, the ions never gain the full energy of the target bias voltage since the dynamic sheath expands and the sheath electric potential changes during the ion flight across the plasma-sheath. Yet, the gas pressure decreases the effects of the ion temperature and the magnetic field.

Although ion temperature has significant effects on the low voltage dynamic sheath, it has almost no effect on the structure of high voltage dynamic sheath. This is because the ion thermal force, in the ion motion equation (3), is weak in comparison with the other forces in the high voltage sheath.

On the other hand, the gas pressure has considerable effects on the sheath dynamic characteristics, because the ion collisional force in the ion motion equation (3) is an important term in the both of low and high voltage sheaths. In other words, unlike the ion thermal force, the ion collisional force grows up by rising the sheath voltage. Therefore, temporal curve of the plasma-sheath characteristics on the target is the same in the low and high voltage sheaths. Calculations show that the gas pressure reduces all of the temporal curves of the target characteristics including, the ion current density, the ion impact energy, the ion incident angle on the target, and the plasma-sheath width in the both of low and high voltage sheath.

ACKNOWLEDGMENTS

This study was supported by Islamic Azad University, Borujerd Branch, Iran. The authors would like to acknowledge the staff of the university.

APPENDIX: IMPLICIT METHOD

The implicit finite difference method overcomes the explicit method difficulties (conditional stability and low precision) at the expense of a somewhat more complicated calculational procedure. For example, according to the implicit method, discretization of Equations (7) and (10) concludes that

$$\frac{N_i^{n+1} - N_i^n}{\Delta t} + \frac{N_{i+1}^{n+1} u_{x,i+1}^{n+1} - N_i^{n+1} u_{x,i}^{n+1}}{\Delta x} = 0, \tag{A1}$$

$$\frac{\phi_{i+1}^{n+1} - 2\phi_i^{n+1} + \phi_{i-1}^{n+1}}{(\Delta x)^2} = \exp\left(\phi_i^{n+1}\right) - N_i^{n+1}, \tag{A2}$$

in which i and n are count space and time steps, respectively. After linearization, relations (A1) and (A2) exchange to

$$A_{1i} N_i^{n+1} + B_{1i} N_{i+1}^{n+1} + C_{1i} u_{x,i}^{n+1} + D_{1i} u_{x,i+1}^{n+1} = E_{1i}, \quad 1 \le i \le n_x - 1, \tag{A3}$$

$$A_{2i} \phi_{i-1}^{n+1} + B_{2i} \phi_i^{n+1} + C_{2i} \phi_{i+1}^{n+1} + D_{2i} N_i^{n+1} = E_{2i}, \quad 2 \le i \le n_x - 1. \tag{A4}$$

Similarly, one can discretize and linearize Equations (11)–(13) to find

$$A_{3i} \phi_i^{n+1} + B_{3i} \phi_{i+1}^{n+1} + C_{3i} N_i^{n+1} + D_{3i} N_{i+1}^{n+1} + E_{3i} u_{x,i}^{n+1} + F_{3i} u_{x,i+1}^{n+1} + G_{3i} u_{z,i}^{n+1} = H_{3i}, \quad 1 \le i \le n_x - 1, \tag{A5}$$

$$A_{4i} u_{x,i}^{n+1} + B_{4i} u_{y,i}^{n+1} + C_{4i} u_{y,i+1}^{n+1} + D_{4i} u_{z,i}^{n+1} = E_{4i} \quad 1 \le i \le n_x - 1, \tag{A6}$$

$$A_{5i} u_{x,i}^{n+1} + B_{5i} u_{y,i}^{n+1} + C_{5i} u_{z,i}^{n+1} + D_{5i} u_{z,i+1}^{n+1} = E_{5i} \quad 1 \le i \le n_x - 1, \tag{A7}$$

where the coefficients $A_{1i}, B_{1i}, \ldots, E_{5i}$ are functions of $\lambda = \Delta t/\Delta x$, N_i^n, $u_{x,i}^n$, $u_{y,i}^n$, $u_{z,i}^n$, and ϕ_i^n. In Equations (A3)–(A7), $i = 1$ and $i = n_x$ introduce the locations of target and plasma pre-sheath interface, respectively, that are the boundaries of simulation zone. Using the boundary conditions $\phi_1^n = \phi_T$, $\phi_{n_x}^n = 0$, $N_{n_x}^n = 1$, $u_{x,n_x}^n = u_{y,n_x}^n = u_{z,n_x}^n = 0$ and initial conditions $\phi_i^1 = 0$, $N_i^1 = 1$, $u_{x,i}^1 = u_{y,i}^1 = u_{z,i}^1 = 0$, these five linear equations can be solved in the n_x points in the simulation zone simultaneously to find the five variables ϕ_i^n, N_i^n, $u_{x,i}^n$, $u_{y,i}^n$, and $u_{z,i}^n$ in these points for each time step.

[1]J. R. Conrad, J. L. Radtke, R. A. Dodd, F. J. Worzala, and N. C. Tran, "Plasma source ion implantation technique for surface modification of materials," J. Appl. Phys. **62**, 4591 (1987).
[2]J. Tendys, I. J. Donnelly, M. J. Kenny, and J. T. A. Pollock, "Plasma immersion ion implantation using plasmas generated by radio frequency techniques," Appl. Phys. Lett. **53**, 2143 (1988).
[3]S. Qin, N. McGruer, C. Chan, and K. Warner, "Plasma immersion ion implantation doping using a microwave multipolar bucket plasma," IEEE Trans. Electron Devices **39**, 2354 (1992).
[4]S. Qin and C. Chan, "Plasma immersion ion implantation doping experiments for microelectronics," J. Vac. Sci. Technol., B **12**, 962 (1994).
[5]N. W. Cheung, "Plasma immersion ion implantation for ulsi processing," Nucl. Instrum. Methods Phys. Res., Sect. B **55**, 811 (1991).
[6]C. A. Pica, M. A. Lieberman, and N. W. Cheung, "Pmos integrated circuit fabrication using bf3 plasma immersion ion implantation," J. Electron. Mater. **21**(1), 75 (1992).
[7]K. F. Sander, "Theory of a thick dynamic positive-ion sheath," J. Plasma Phys. **3**, 353 (1969).
[8]M. A. Lieberman and A. J. Lichtenberg, *Principles of Plasma Discharges and Materials Processing*, 2 ed. (John Wiley and Sons, Inc., New York, 1994).

[9]P. K. Chu, S. Qin, C. Chan, N. W. Cheung, and L. A. Larson, "Plasma immersion ion implantation - A fledgling technique for semiconductor processing," Mater. Sci. Eng., R **17**(6), 207 (1996).
[10]M. A. Lieberman, "Model of plasma immersion ion implantation," J. Appl. Phys. **66**, 2926 (1989).
[11]L. Minghao, Z. Yu, D. Wanyu, L. Jinyuan, and W. Xiaogang, "Effects of ion temperature on collisionless and collisional rf sheath," Plasma Sci. Technol. **8**(5), 544 (2006).
[12]G. C. Das, B. Singha, and J. Chutia, "Characteristic behavior of the sheath formation in thermal plasma," Phys. Plasmas **6**(9), 3685 (1999).
[13]B. Alterkop, S. Goldsmith, and R. L. Boxman, "Presheath in fully ionized collisional plasma in a magnetic field," Contrib. Plasma Phys. **45**(7), 485 (2005).
[14]M. Khoramabadi, H. Ghomi, and P. K. Shukla, "The bohm-sheath criterion in plasmas containing electrons and multiply charged ions," J. Plasma Phys. **79**, 267 (2013).
[15]H. Ghomi, M. Khoramabadi, P. K. Shukla, and M. Ghorannevis, "Plasma sheath criterion in thermal electronegative plasmas," J. Appl. Phys. **108**, 063302 (2010).
[16]H. Ghomi and M. Khoramabadi, "Influence of ion temperature on plasma sheath transition," J. Plasma Phys. **76**, 247 (2010).
[17]M. Khoramabadi, H. Ghomi, and P. K. Shukla, "Numerical investigation of the ion temperature effects on magnetized dc plasma sheath," J. Appl. Phys. **109**, 073307 (2011).
[18]N. N. Safa, H. Ghomi, M. Khoramabadi, S. Ghasemi, and A. R. Niknam, "External magnetic field effect on the sheath dynamics and implantation profiles in the vicinity of a long step shaped target in plasma immersion ion implantation," Vacuum **101**, 354 (2014).
[19]B. Carnahan, H. A. Luther, and J. O. Wilkes, *Applied Numerical Methods* (John Wiley and Sons, Inc., New York, 1990).
[20]R. N. Franklin, "The plasma-sheath and its stability in a quiescent plasma containing two species of positive ion," J. Phys. D: Appl. Phys. **36**, 1806 (2003).
[21]R. N. Franklin, "Where is the sheath edge?," J. Phys. D: Appl. Phys. **37**, 1342 (2004).
[22]Z. L. Dai and Y. N. Wang, "Simulations of ion transport in a collisional radio-frequency plasma sheath," Phys. Rev. E **69**, 036403 (2004).
[23]R. N. Franklin, "The plasma -sheath boundary region," J. Phys. D: Appl. Phys. **36**, R309 (2003).
[24]U. K. Riamann, "Theory of the collisional presheath in an oblique magnetic field," Phys. Plasmas **1**(3), 552 (1994).
[25]X. B. Tian and P. K. Chu, "Electrochemical corrosion properties of aisi304 steel treated by low-temperature plasma immersion ion implantation," Scr. Mater. **43**(5), 417 (2000).
[26]X. B. Tian, C. B. Wei, S. Q. Yang, R. K. Y. Fu, and P. K. Chu, "Corrosion resistance improvement of magnesium alloy using nitrogen plasma ion implantation," Surf. Coat. Technol. **198**, 454 (2005).
[27]K. G. Kostov, J. J. Barroso, and M. Ueda, "Two dimensional computer simulation of plasma immersion ion implantation," Braz. J. Phys. **34**(4B), 1689–1695 (2004).
[28]B. P. Wood, "Displacement current and multiple pulse effects in plasma source ion implantation," J. Appl. Phys. **73**, 4770 (1993).
[29]C. Corbella, M. Rubio-Rov, E. Bertran, S. Portal, E. Pascual, M. C. Polo, and L. J. Andujar, "Ion energy distributions in bipolar pulsed-dc discharges of methane measured at the biased cathode," Plasma Sources Sci. Technol. **20**, 015006 (2011).
[30]C. Blawert, B. L. Mordike, G. A. Collins, K. T. Short, and J. Tendys, "Influence of process parameters on the nitriding of steels by plasma immersion ion implantation," Surf. Coat. Technol. **103–104**, 240 (1998).